Analytic model for the electrowetting properties of oil-water-solid systems

A. Cavalli, B. Bera, D. van den Ende, and F. Mugele
Physics of Complex Fluids, MESA+Institute of Technology, University of Twente, PO Box 217, 7500AE, The Netherlands
(Received 2 January 2016; published 13 April 2016)

The competitive wetting of oil and aqueous electrolytes on solid surfaces depends strongly on the surface charge of the solid-water and the water-oil interface. This charge density is generally not known *a priori* but changes as ions adsorb or desorb from or to the interfaces, depending on the composition of the fluid and the thickness of thin films of the aqueous phase that frequently arise on hydrophilic surfaces, such as minerals. We analyze the wettability of such systems by coupling standard Derjaguin-Landau-Verwey-Overbeek theory to a linearized charge regulation model. The latter is found to play an important role. By linearizing electrostatic interactions as well, we obtain a fully analytic description of transitions between different wetting scenarios as a function of the surface potentials at infinite separation and the charge regulation parameters of the two interfaces. Depending on the specific values of the regulation parameters, charge regulation is found to extend the parameter range of partial wetting and complete wetting at the expense of pseudopartial wetting and metastable wetting configurations, respectively. A specific implementation of the model is discussed for mica-water-alkane systems that was investigated in recent experiments.

DOI: 10.1103/PhysRevE.93.042606

I. INTRODUCTION

Solid surfaces immersed in aqueous electrolytes typically acquire a finite surface charge due to adsorption and desorption of ions, including protons. The surface charge attracts counterions from the solution leading to the formation of an electric double layer at the solid-electrolyte interface. Many phenomena in colloid, soft matter, and interfacial science are governed by the interaction forces that arise when two interfaces approach each other such that their electric double layers begin to overlap. Such electric double-layer forces have been studied in great detail in various contexts, including, in particular, colloidal stability, surface forces, foam stability, and wetting. In classical Derjaguin-Landau-Verwey-Overbeek (DLVO) theory, the electrostatic disjoining pressure, i.e., the electrostatic interaction force per unit area, depends on the distribution of the ions and the electrostatic potential between the two interacting surfaces [1,2]. Both are controlled indirectly by the charge (or the potential) on the two interfaces, which enters the calculation of the electric potential distribution as a boundary condition. Because of this indirect control and the thermal equilibration of the counterions in the diffuse part of the double layer, electric double-layer forces display a richer behavior than bare electrostatic interactions in vacuum. For example, interfaces with constant charges of opposite sign always attract each other in vacuum. However, in an electrolyte medium, the force between these interfaces is only attractive at sufficiently large distance, but becomes repulsive upon close approach, unless the two opposing surface charge densities are exactly of the same magnitude (see, e.g., Refs. [1,3]). For the calculation of surface forces, classical textbooks typically treat either the surface charge or the surface potential as constant upon varying the distance between the two interfaces [1,2]. However, measurements of surface force with the surface forces apparatus (SFA) [4,5] and with the atomic force microscope (AFM) [6,7] have shown that the actual forces typically fall in between the limits of constant charge and the constant potential boundary conditions. This deviation is caused by the fact that usually neither the charges nor the potentials remain constant upon varying the thickness of a thin electrolyte film. Increasing double-layer overlap changes the local concentration of ions at the two interfaces and thereby shifts the chemical adsorption equilibria of ions and thus the surface charge. This phenomenon, known as charge regulation, was analyzed for the first time in detail by Ninham and Parsegian [8]. A proper calculation of electric double-layer forces therefore requires a self-consistent calculation of both electric potential distribution and surface charge density. The exact analytical solution for two identical surfaces presented by Ninham and Parsegian has later between extended to the general case of two dissimilar surfaces with dissimilar charge regulation properties by Behrens and Borkovec [9].

In the present work, we are interested in the interaction forces between two dissimilar surfaces, namely a solid-water interface and a water-air or water-oil interface. While the details of the charging mechanisms of water-air and water-oil interfaces are generally less well understood than in the case of solid-water interfaces, the conceptual framework of calculating the electrostatic interaction forces is the same as in the case of two solid-liquid interfaces approaching each other. Although the exact analytical solutions of the Poisson-Boltzmann equation for charge regulating surfaces are very elegant, their expression in terms of Jacobian elliptic integrals is rather complex and nonintuitive [8,9]. Therefore, following Carnie and Chan [10], we resort to the simpler linearized regime for our present analysis, in which we linearize both the Poisson-Boltzmann equation to the Debye-Hückel equation and the charge regulation problem. While applied widely in the context of surface force measurements, systematic studies of the consequences of surface charges and variations thereof for wetting are rather scarce [11–14] and frequently focused on the thickness and stability of thin wetting films. Recent theoretical studies analyzed the impact of surface charges on the order of wetting transitions [15,16]. Possibly, the effect of electrostatic interactions has frequently been overlooked because the absolute values of the electrostatic interaction energies are typically only of the order of a few mJ/m^2 and thus much smaller than common surface tension forces of chemical interaction. (An exception to this

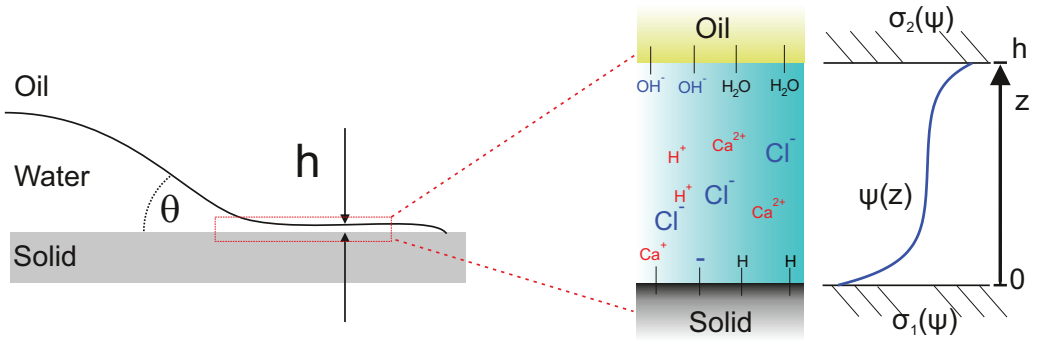

FIG. 1. Sketch of the system of interest, and corresponding electrostatic description.

rule is electrowetting, where the electric fields are spread over an artificially thick insulating layers [17].) Nevertheless, it was recently reported [14] that certain mineral-water-oil systems, specifically mica-water-decane, display a transition from (almost) complete water wetting to partial wetting upon adding sufficient amounts of divalent Ca^{2+} or Mg^{2+} ions to the aqueous phase. This transition is believed to play an important role in modern enhanced oil recovery techniques, in particular, in so-called low salinity water flooding [18–20]. The experiments suggested that the transition is driven by a reversal of the charge of the mica-water interface upon adsorption of divalent cations. This interpretation was supported by calculations of the interaction energies including an empirical expression for short-range chemical forces, and standard expressions from DLVO theory for van der Waals and electrostatic interactions. Yet, the latter was calculated for the simplified constant charge boundary condition and ignored the possibility of charge regulation. The purpose of the present work is to extend that previous model and to explore the consequences of charge regulation for the wettability of such systems. To this end, we recapitulate the formalism developed by Carnie and Chan and others [10,21] in the first part of this work and calculate the electrostatic interaction energy per unit area between the two adjacent interfaces. Subsequently, we interpret this interaction energy as an effective interface potential to evaluate the consequences for the wettability of the system in the context of an interface displacement model [22,23]. We identify four generic shapes of the interface potential, corresponding to complete wetting, partial wetting, pseudopartial wetting, and a metastable wetting film. Finally, we discuss the occurrence of these four scenarios in the parameter space that is given by the surface charge densities and the so-called (charge) regulation parameters of the two interfaces involved. In the Appendix, we provide an explicit implementation of the general model for a specific example of surface speciation reactions as applicable for mica-water-alkane systems.

II. MODEL

In the following we consider the system sketched in Fig. 1. The solid phase is kept in ambient oil, where the intruding aqueous phase forms a drop of contact angle θ. Irrespective of the magnitude of θ, which is 0 for a complete wetting situation and >0 for pseudopartial wetting, there is a water film of thickness h, containing different ionic species, sandwiched between the solid substrate and the oil bath. Both the solid-water and the water-oil interfaces [24] can bind charged species, thus acquiring surface charge densities $\sigma_1(\phi)$ and $\sigma_2(\phi)$, respectively. It is worth noticing that these surface charges depend on the electrostatic potential, which in turn affects the ionic concentration in the proximity of each substrate. These interfaces are thus known as charge regulating, as their charge is regulated by the electrostatic potential.

At low ionic concentrations,[1] this system can be appropriately described by the Poisson-Boltzmann equation.

$$\frac{\partial^2\phi}{\partial z^2} = \frac{-e}{\epsilon\epsilon_0}\sum_i Z_i[n_\infty]_i e^{-Z_i e\phi/k_B T} \tag{1a}$$

$$\left.\frac{\partial\phi}{\partial z}\right|_{z=0} = -\frac{\sigma_1(\phi)}{\epsilon\epsilon_0} \tag{1b}$$

$$\left.\frac{\partial\phi}{\partial z}\right|_{z=h} = \frac{\sigma_2(\phi)}{\epsilon\epsilon_0}. \tag{1c}$$

Here e is the electron charge, ϵ and ϵ_0 the relative permittivity of water and vacuum permittivity, respectively, Z_i the valency of the ith ionic species, $[n_\infty]_i$ the bulk concentration of the ith ionic species (in molecules m^{-3}), k_B the Boltzmann constant, and T the temperature. Charge neutrality in the bulk introduces the further constraint $\sum_i Z_i[n_\infty]_i = 0$. Note that the surface charge densities σ_1 and σ_2, that appear here as boundary conditions for the Poisson-Boltzmann equation, are required to be determined self-consistently as a part of the solution procedure, as described in detail below. Defining the ionic strength as $I_\infty = \frac{1}{2}\sum_i Z_i^2[n_\infty]_i$ and the ionic fraction as $x_i = \frac{[n_\infty]_i}{2I_\infty}$, we can write Eqs. (1a), (1b), and (1c) in dimensionless form:

$$\frac{\partial^2\psi}{\partial\zeta^2} = -\sum_i Z_i x_i e^{-Z_i\psi} \tag{2a}$$

$$\left.\frac{\partial\psi}{\partial\zeta}\right|_{\zeta=0} = -q_1(\psi) \tag{2b}$$

$$\left.\frac{\partial\psi}{\partial\zeta}\right|_{\zeta=\kappa_D h} = q_2(\psi). \tag{2c}$$

[1]So that ion-ion interactions can be neglected, and each ion is only affected by the mean electrostatic field.

Here $\zeta = \kappa_D z$, $\psi = e\phi/k_B T$ and $\sigma(\phi) = 2eI_\infty \kappa_D^{-1} q(\psi)$. The reciprocal Debye length is given by:

$$\kappa_D = \sqrt{\frac{2I_\infty e^2}{\epsilon\epsilon_0 k_B T}}. \tag{3}$$

It is easy to imagine that these highly nonlinear equations can only be approached analytically under some simplifying assumptions. For instance, in the large separation limit $\kappa_D h \gg 1$, Grahame equation [1] can be obtained integrating Eq. (2a) once:

$$\frac{\partial \psi}{\partial \zeta} = \pm \sqrt{\sum_i 2x_i (e^{-Z_i \psi} - 1)}. \tag{4}$$

Equating Eqs. (2b) and (4) allows us to calculate the surface charge $q_{1,\infty}(\psi_{1,\infty})$ at infinite separation.

In the limit $\psi \ll 1$, we can Taylor expand the exponential term in Eq. (2a), $e^{-Z_i \psi} \simeq 1 - Z_i \psi$. If we further employ the charge neutrality condition, we obtain the linear Debye-Huckel (DH) equation,

$$\frac{\partial^2 \psi}{\partial \zeta^2} = \psi. \tag{5}$$

The choice of the Debye-Huckel approximation allows two dramatic simplifications of the problem. First, the equation keeps the same form for an arbitrary mixture of $(m{:}n)$ electrolytes, as the contribution of the different species appears only through the ionic strength in κ_D. Second, it is easy to find a suitable ansatz for the electrostatic potential in the electrolyte between the interfaces,

$$\psi(\zeta) = Ae^{-\zeta} + Be^{\zeta - \kappa_D h}. \tag{6}$$

Despite the significant simplification introduced by linearizing the PB equation, the charge regulation boundary conditions prevent us from finding an analytic expression for the coefficients A and B in Eq. (6). Generally speaking $q_{1,2}(\psi)$ are nonlinear functions, and solving Eq. (5) and (2b)–(2c) requires a numerical step. An order zero approximation would be to assume that each interface keeps its charge at infinite separation, i.e., $q_i(\psi) = q_{i\infty}$. This so-called constant charge assumption is widely applied but in fact rather crude, as it neglects any effect from the other interface. Following Refs. [10,25], we therefore take a step further, and consider the linearized approximation:

$$q_i(\psi) = q_{i\infty} + \left.\frac{\partial q}{\partial \psi}\right|_{\psi=\psi_{i,\infty}} (\psi - \psi_{i,\infty}). \tag{7}$$

We thus allow the charge of each interface to vary linearly around its equilibrium value at infinite separation, as a consequence of the proximity of the other substrate. If we momentarily leave the nondimensional formulation, we see that the units of the parameter $\left.\frac{\partial \sigma}{\partial \phi}\right|_{\phi=\phi_{i,\infty}} = \epsilon\epsilon_0 \kappa_D \left.\frac{\partial q}{\partial \psi}\right|_{\psi=\psi_{i,\infty}}$ are those of a capacitance, describing the sensitivity of the surface charge to a change in the local potential, which is sometimes denoted as regulation capacitance [10] or a surface buffer capacitance [26]. In the following, we will denote the nondimensional form of this capacitance as $K_i = -\left.\frac{\partial q}{\partial \psi}\right|_{\psi=\psi_{i,\infty}}$. With this definition, a constant charge boundary condition corresponds to $K_i = 0$, while we recover the constant potential behavior for $K_i^{-1} = 0$.

The linearization of the boundary conditions makes our system of equations suitable for an analytic solution. Solving Eq. (5) with the ansatz of Eq. (6) and the boundary conditions from Eq. (7), we obtain the following expression for the electrostatic potential in the film (as originally derived by Carnie and Chan) [10]:

$$\psi(\zeta) = \frac{\psi_{2,\infty} - \Delta_2 \psi_{1,\infty} e^{-\kappa_D h}}{1 - \Delta_1 \Delta_2 e^{-2\kappa_D h}} e^{-(\kappa_D h - \zeta)} + \frac{\psi_{1,\infty} - \Delta_1 \psi_{2,\infty} e^{-\kappa_D h}}{1 - \Delta_1 \Delta_2 e^{-2\kappa_D h}} e^{-\zeta}, \tag{8}$$

where the parameter Δ_i is given by $\frac{K_i - 1}{K_i + 1}$. We therefore have that $\Delta_i = 1$ denotes the constant surface potential boundary condition and $\Delta_i = -1$ represents the constant surface charge boundary condition. Notice that both coefficients A and B depend on the potentials at infinite separation $\psi_{1\infty}$ and $\psi_{2\infty}$. This confirms that the total electrostatic potential is not just a linear superposition of the potentials for each isolated interface, and depends on the proximity h of the other substrate. Interestingly, for $\Delta_{1,2} = 0$, we recover the linear superposition result.

The reader may wonder if this linearization procedure is suitable to describe solid-water-oil systems. To answer this question, we need to discuss the structure of the $\sigma(\psi)$ curve for the interfaces under consideration. Water-solid interfaces are often described in terms of a complexation model [28], which accounts for the binding of different ionic species to the substrate. For instance, a mica-water interface in the presence of a single ionic species can be described by the reactions

$$S \equiv \mathrm{H} \rightleftharpoons S^- + \mathrm{H}^+ \tag{9a}$$

$$S \equiv \mathrm{C}^{Z_c - 1} \rightleftharpoons S^- + C^{Z_c}. \tag{9b}$$

In this model, each surface site S can bind a proton H^+ or a cation C^{Z_c}. This results in a distinct profile for the $\sigma(\psi)$ function, which is sketched in Fig. 2(a). $\sigma(\psi)$ shows two plateaus, corresponding to a fully deprotonated substrate, with charge $\sigma_{\min}$, and a fully saturated one, of charge $\sigma_{\max}$. As the dashed red line shows, this kind of behavior can be quite accurately captured by a piecewise linear approximation, with two constant-charge ($\Delta = -1$) regions and a linear transition among them. The surface charge at the oil-water interface has been the subject of extensive debate [24,29]. A general consensus has been achieved over two aspects: first, an oil-water interface is negatively charged at pH larger than 3–4 [30]. Second, the oil-water interface shows weak ionic (particularly anionic) adsorption. These observation are consistent with an enhanced water autolysis at the oil-water interface, described by Eq. (A8):

$$S \equiv \mathrm{H_2O} \rightleftharpoons S \equiv \mathrm{OH}^- + \mathrm{H}^+ \tag{10}$$

and resulting in the surface charge profiles shown in Fig. 2(b). According to this description, the oil-water interface is neutral at large negative potentials, and develops a negative charge for increasing positive potential. For both interfaces, the details of $\sigma(\psi)$ depend of course on the specific chemistry of the surface,

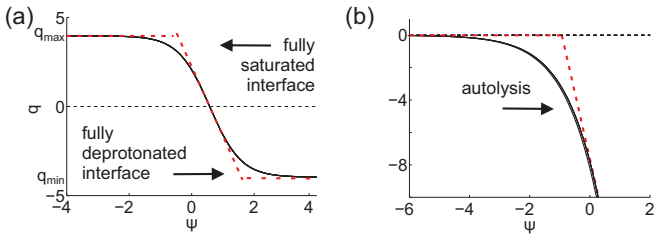

FIG. 2. (a) $\sigma(\psi)$ profile for the mica-water interface, based on the complexation model from Eqs. (9). The adsorption coefficients are $pK_H = 4$ and $pK_{Ca^{2+}} = 1.5$, for site density $\Gamma_{mica} = 0.8$ sites/nm^2 [27]. (b) $\sigma(\psi)$ profile for the oil-water interface, based on the complexation model from Eq. (10). The autolysis reaction coefficient is $pK_H = 7$, for site density $\Gamma_{oil} = 17.3$ sites/nm^2 [24]. All ψ values are taken at the surface. Both curves are obtained for pH = 6 and Ca^{2+} bulk concentration $[Ca^{2+}]_\infty = 100$ mM. The surface charge at mica-water interface in (a) is positive because of strong cation adsorption at this high salt concentration. Details on the derivation of these curves can be found in the Appendix.

i.e., the equilibrium constant for each adsorption/desorption reaction. However, the character of these curves, with plateaus connected by sharp transitions, is rather universal, and can be traced back to the Langmuir adsorption theory [31] underlying these surface chemistry models. The value of σ_∞ then determines which linear regime is relevant for the system. In the Appendix, we discuss how to relate the surface chemistry parameters to ψ_∞ and Δ, providing quantitative examples.

III. INTERMEZZO: INTERFACE POTENTIAL AND WETTING CONFIGURATIONS

Equation (8) allows us to calculate the electrostatic energy density per unit volume inside the film. This quantity, known as disjoining pressure, is given by:

$$\Pi_{el}(h) = 4\left[\psi^2 - \frac{1}{2}\left(\frac{\partial\psi}{\partial\zeta}\right)^2\right] = 4\left[\frac{2\psi_{1,\infty}\psi_{2,\infty}e^{-\kappa_D h} - [\Delta_1\psi_{2,\infty}{}^2 + \Delta_2\psi_{1,\infty}{}^2]e^{-2\kappa_D h}}{(1-\Delta_1\Delta_2 e^{-2\kappa_D h})^2} - \frac{\psi_{1,\infty}\psi_{2,\infty}e^{-\kappa_D h}}{1-\Delta_1\Delta_2 e^{-2\kappa_D h}}\right]. \quad (11)$$

A positive disjoining pressure leads to a thicker film, a negative value to a thinner one. The electrostatic interaction potential per unit area is given by:

$$\Phi_{el}(h) = -\int_\infty^{\kappa_D h} \Pi_{el}(\zeta)d\zeta = \frac{2\psi_{1,\infty}\psi_{2,\infty}e^{-\kappa_D h} - \left[\Delta_1\psi_{2,\infty}^2 + \Delta_2\psi_{1,\infty}^2\right]e^{-2\kappa_D h}}{1-\Delta_1\Delta_2 e^{-2\kappa_D h}} \quad (12)$$

$\Phi_{el}(h)$ describes the electrostatic energy per unit area in the film as a function of its thickness. $\Phi_{el}(h)$ and $\Pi_{el}(h)$ thus provide the key information on the wetting behavior of the system. Please note that Φ_{el} can be dimensionalized by multiplying with the factor k_BT/e. Equations (11) and (12) are deceptively compact, as they can lead to four qualitatively distinct types of wetting behaviors, depending on the values of $\psi_{1,\infty}, \psi_{2,\infty}, \Delta_1$ and Δ_2. In the next section we will analyze in details how these parameters affect $\Phi_{el}(h)$. Before doing so, however, we first discuss the connection between $\Phi_{el}(h)$ and the wetting properties of the system, which we show in Fig. 3.

Figure 3(a) shows an asymptotically repulsive interface potential. The minimum energy configuration is attained for $h \to \infty$. This corresponds to a complete wetting scenario. Figure 3(b) shows an interface potential with a minimum at a finite thickness h_{min}, and an attractive convex profile for large h. If the interface potential is convex, it is thermodynamically advantageous for a film of thickness h_0 to split into two films of thicknesses h_1 and h_2 covering fractions α_1,α_2 of the substrate, so that $\alpha_1 + \alpha_2 = 1$. Due to convexity, we indeed have $(\alpha_1 + \alpha_2)\Phi(h_0) > \alpha_1\Phi(h_1) + \alpha_2\Phi(h_2)$. Any film of thickness larger than h_{min} will thus spontaneously evolve into a macroscopic droplet ($h \to \infty$) in equilibrium with a thin film of thickness h_{min} [23]. The equilibrium contact angle θ_{eq} can be found considering the horizontal force balance at the edge of the drop, which reads (in dimensional representation):

$$\gamma + \Phi_{el}(h_{min}) = \gamma\cos\theta_{eq} \to \gamma(1-\cos\theta_{eq}) = -\Phi_{el}(h_{min}). \quad (13)$$

Notice also how the slope of $\Phi_{el}(h)$, and thus the disjoining pressure $\Pi_{el}(h)$, is the same at $h = h_{min}$ and $h \to \infty$, which allows the two films of different thickness to coexist. Figure 3(c) shows an asymptotically attractive concave potential. This scenario is analogous to Fig. 3(b), with $h_{min} = 0$. Part of the film dries up ($h = 0$), and part forms a macroscopic droplet ($h \to \infty$). We thus obtain a partial wetting configuration. Finally, we consider the interface potential in Fig. 3(d). which exhibits a long-range repulsion and a short-range attraction. The associated wetting configuration is metastable. Depending on its initial thickness, a film will evolve into a completely wetting layer or a partial wetting droplet.

IV. PHASE-SPACE ANALYSIS

We now discuss how these four different wetting configurations arise for varying boundary and charge regulation conditions. First, we rewrite the disjoining pressure as

$$\Pi_{el}(h) = 4\frac{e^{-\kappa_D h}}{(1-\Delta_1\Delta_2 e^{-2\kappa_D h})^2}\left[\psi_{1,\infty}\psi_{2,\infty} + \Delta_1\Delta_2\psi_{1,\infty}\psi_{2,\infty}e^{-2\kappa_D h} - \left[\Delta_1\psi_{2,\infty}^2 + \Delta_2\psi_{1,\infty}^2\right]e^{-\kappa_D h}\right]. \quad (14)$$

The sign of $\Pi_{el}(h)$ is uniquely defined by the term in square brackets, which is a quadratic polynomial in $x = e^{-\kappa_D h}$, $\pi(x) = [\psi_{1,\infty}\psi_{2,\infty} + \Delta_1\Delta_2\psi_{1,\infty}\psi_{2,\infty}x^2 - [\Delta_1\psi_{2,\infty}^2 + \Delta_2\psi_{1,\infty}^2]x]$. The roots of $\pi(x)$ are $x_\pm = \{\frac{\psi_{2,\infty}}{\Delta_2\psi_{1,\infty}}, \frac{\psi_{1,\infty}}{\Delta_1\psi_{2,\infty}}\}$. The corresponding equilibrium film thicknesses are thus $h_\pm = \{\kappa_D^{-1}\ln\frac{\Delta_2\psi_{1,\infty}}{\psi_{2,\infty}}, \kappa_D^{-1}\ln\frac{\Delta_1\psi_{2,\infty}}{\psi_{1,\infty}}\}$. This information allows us to draw some very general conclusions. If either $h_+ > 0$ or $h_- > 0$, the interface potential exhibits

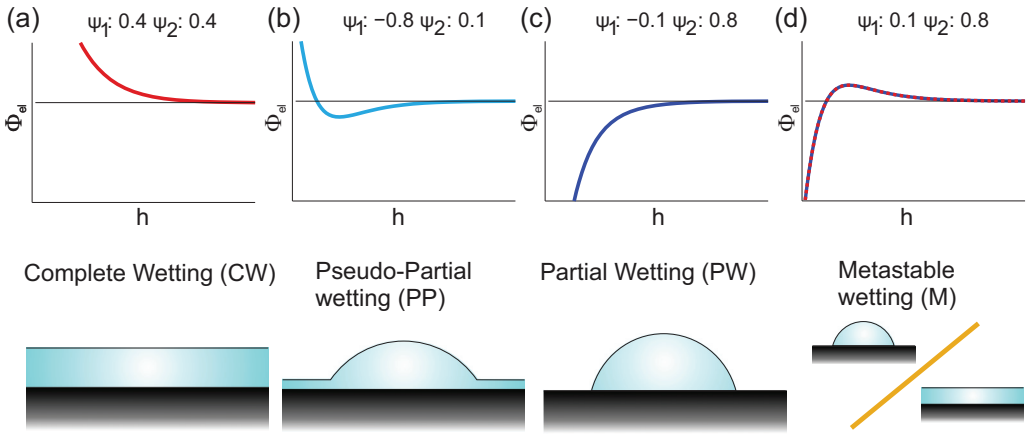

FIG. 3. The four interface potential $\Phi_{el}(h)$ predicted by our model, with corresponding wetting configurations: (a) complete wetting (CW, red); (b) pseudopartial wetting (PP, light blue), (c) partial wetting (PW, dark blue), and metastable wetting (M, red-blue stripes). All interface potentials are computed for $\Delta_1 = 0.5$, $\Delta_2 = -0.5$, and the values of ψ_∞ shown for each curve.

one local extremum. Note that both solutions cannot be positive at the same time, as it would imply $\Delta_1\Delta_2 > 1$, which is impossible by construction. The interface potential will thus show at most one local maximum or minimum. As $\Phi_{el}(\infty) = 0$, it is sufficient to check the sign of the potential at $h = 0$ to distinguish between the two. If h_+ and h_- are both negative, $\Phi_{el}(h)$ is monotonously attractive or repulsive. Again, it is sufficient to check the sign of $\Phi_{el}(0)$ to discriminate the latter two scenarios.

1. Constant-charge and constant-charge-like interfaces: $\Delta_{1,2} < 0$

We first consider the case $\Delta_{1,2} < 0$. As an example, Fig. 4 shows the possible wetting configuration for $\psi_{1,\infty}, \psi_{2,\infty} \in [-1,1]$, when [Fig. 4(a)] $\Delta_1 = \Delta_2 = -1$, (i.e., both surfaces display constant charge behavior), and [Fig. 4(b)] $\Delta_1 = -0.75$, $\Delta_1 = -0.5$, (i.e., both surfaces are weakly charge regulating, closer to constant charge). If the charge of the two substrates at infinite separation have the same sign, $\text{sign}(\psi_{1,\infty}) = \text{sign}(\psi_{2,\infty})$, one can easily check that $\Pi_{el}(h)$ is always positive. The interaction of the interfaces is thus always repulsive, leading to a complete wetting configuration. If $\text{sign}(\psi_{1,\infty}) \neq \text{sign}(\psi_{2,\infty})$, $\Phi_{el}(h)$ shows a local minimum

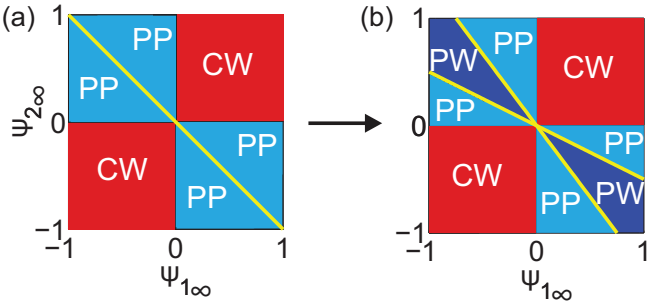

FIG. 4. Phase-space maps for (a) $\Delta_1 = \Delta_2 = -1$, and (b) $\Delta_1 = -0.75$, $\Delta_2 = -0.5$. The color coding is as in Fig. 3, i.e., red for complete wetting (CW), dark blue for partial wetting (PW), and light blue for pseudopartial wetting (PP).

for $\psi_{1,\infty} > \psi_{2,\infty}/\Delta_2$ and $\psi_{1,\infty} < \Delta_1\psi_{2,\infty}$. For $\Delta_1\psi_{2,\infty} < \psi_{1,\infty} < \psi_{2,\infty}/\Delta_2$, the interface potential is monotonously attractive, leading to a partial wetting configuration. We can get a physical picture of these results starting from the extreme case of constant charge at both interfaces, $\Delta_{1,2} = -1$. In this case, the surface charge of each interface is not affected by the proximity of the other one. This explains the repulsion between interfaces of same-sign surface charge, and long-range attraction between opposite-sign interfaces. However, when surface charges of different magnitude and sign are brought together, a net charge will be localized between them, leading to a strong imbalance of the local ionic concentration. Osmotic pressure will thus oppose the further approach of the interfaces, generating a strong short-range repulsion. For this reason, constant charge interfaces exhibit (true) partial wetting only when $\psi_{1\infty} = -\psi_{2\infty}$. In this case, the two surface charges match exactly, leading to zero net charge when the interfaces are brought together. For the more general case $-1 < \Delta_{1,2} < 0$, a wider region of partial wetting configurations appears, as the interfaces will charge regulate to match their magnitude at short separation, in order to avoid the energy-expensive configuration with localized charge in a thin film. Whether the charge regulation results in a pseudopartial or partial wetting configuration depends on $\Delta_{1,2}$ and the imbalance $\psi_{1\infty} - \psi_{2\infty}$. Large imbalances, and $\Delta_{1,2}$ close to 1, lead to a stronger short-range repulsion and thus more pseudopartial wetting.

2. Constant-potential and constant-potential-like interfaces: $\Delta_{1,2} > 0$

If the potential of the two substrates at infinite separation has opposite sign, we see that $\Pi_{el}(h)$ is always negative. The interaction of the interfaces is thus always attractive, leading to a partial wetting configuration. If the charge of the interfaces at infinite separation has the same sign, we observe a local maximum in $\Phi(h)$ for $\psi_{1,\infty} > \psi_{2,\infty}/\Delta_2$ and $\psi_{1,\infty} < \Delta_1\psi_{2,\infty}$. As discussed in relation to Fig. 3, this range corresponds to a metastable wetting configuration, which can evolve into a partial or a complete wetting state depending on the initial thickness of the film. For $\Delta_1\psi_{2,\infty} < \psi_{1\infty} < \psi_{2,\infty}/\Delta_2$, the interface potential is monotonously repulsive, leading to a

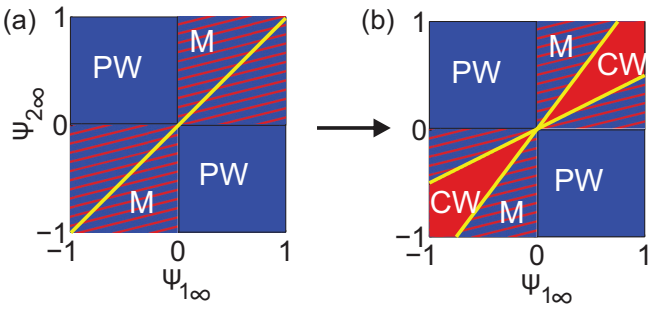

FIG. 5. Phase-space maps for (a) $\Delta_1 = \Delta_2 = +1$, and (b) $\Delta_1 = +0.75$, $\Delta_2 = +0.5$. The color coding is as in Fig. 3, i.e., red for complete wetting (CW), dark blue for partial wetting (PW), and red-blue stripes for a metastable wetting (M) state.

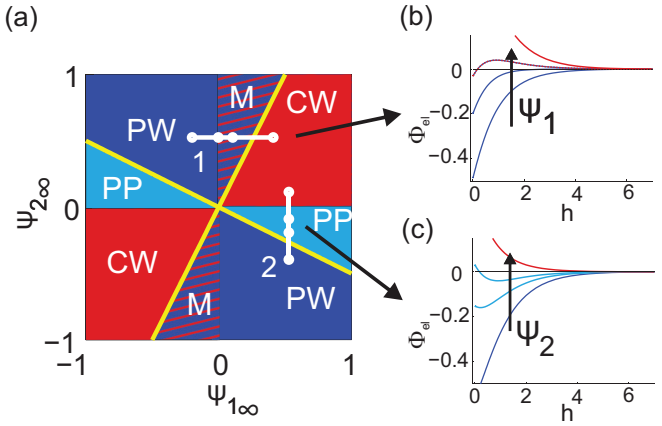

FIG. 6. (a) Phase-space maps for $\Delta_1 = +0.5$, $\Delta_2 = -0.5$. The color coding is as in Fig. 3, i.e., red for complete wetting (CW), dark blue for partial wetting (PW), light blue for pseudopartial wetting (PP), and red-blue stripes for a metastable wetting (M) state. The two wetting transitions discussed in the main text are shown as white lines, and labeled "1" and "2". (b) Interface potential for selected configurations along path 1, complete wetting, red (top) curve; metastable wetting (red-blue stripes, second curve from top), followed by partial wetting (dark blue, bottom two curves). (c) Interface potential for selected configurations along path 2, complete wetting, red (top) curve; pseudopartial wetting (light blue, second and third curve from top), followed by partial wetting (dark blue, bottom curve).

complete wetting configuration. Once again, we can get a physical understanding of these results starting from the constant potential case $\Delta_{1,2} = 1$ [Fig. 5(a)], and generalizing some trends for $1 > \Delta_{1,2} > 0$ [Fig. 5(b)]. It is convenient to discuss the long- ($\kappa_D h \gg 1$) and short-range ($\kappa_D h \ll 1$) interactions separately. For $\kappa_D h \gg 1$, the character of the interface potential is largely defined by the sign of the surface charge at infinite separation. We thus observe attraction for opposite-sign surface charges, and repulsion for same-sign ones. For $\kappa_D h \ll 1$, the electrolyte screening is much less relevant. The two interfaces are kept at constant potential, and thus act like the plates of a capacitor. If $\psi_{1\infty} \neq \psi_{2\infty}$ an electric field develops between them, whose intensity diverges while the interfaces get closer, even if $\psi_{1,\infty}$ and $\psi_{2,\infty}$ have the same sign. This leads to a diverging attractive interaction for any case but $\psi_{1\infty} = \psi_{2\infty}$. Once again, charge regulation softens this behavior and leads to a wider range of complete wetting. In Fig. 5(b) we plot the possible wetting configurations for $\psi_{1,\infty}, \psi_{2,\infty} \in [-1,1]$, when $\Delta_1 = 0.75$, and $\Delta_2 = 0.5$. We observe that a complete-wetting branch opens around the $\psi_{1\infty} = \psi_{2\infty}$ line. This is because the charge at the interfaces regulates to reduce the strength of the electric field, and thus avoid the divergent behavior of the constant-potential case. Whether this leads to a finite attractive interaction at short range, or even a repulsive one depends again on the $\Delta_{1,2}$ and the imbalance $\psi_{1\infty} - \psi_{2\infty}$.

3. A mixed situation: $\Delta_1 = 0.5$, $\Delta_2 = -0.5$

The previous sections have shown how a rich wetting space arises even among alike interfaces. In Fig. 6 we show a rather complex scenario, where $\psi_{1,\infty}, \psi_{2,\infty} \in [-1,1]$, and $\Delta_1 = 0.5$, $\Delta_2 = -0.5$. One can see that, for this choice of boundary conditions, all four wetting configurations introduced earlier are accessible. It is therefore interesting to consider the different wetting transitions that could be observed for this system. Let us consider path 1 in Fig. 6(a), which begins from point $\psi_{1,\infty} = -0.2, \psi_{2,\infty} = 0.5$, corresponding to a partial wetting state. If we increase $\psi_{1,\infty}$ while keeping $\psi_{2,\infty}$ fixed, we move rightward in the phase space into a metastable wetting region. The system will remain in a partial wetting state, as that is one of the allowed equilibria in this region. Moving even further, upon crossing the $\psi_{1\infty} = \psi_{2\infty}/\Delta_2$ line, the system evolves into a completely wetted state. If we now move back along the same path, we will observe an hysteretic effect. Inside the metastable region, the system will remain in the completely wetted state, which is the other allowed equilibrium. However, when $\psi_{1\infty}$ becomes negative, we recover the partial wetting state. Let us now consider path 2 in Fig. 6(a), which begins from point $\psi_{1,\infty} = 0.5, \psi_{2,\infty} = -0.4$, also corresponding to a partial wetting state. We now fix the value of $\psi_{1,\infty}$, and increase $\psi_{2,\infty}$ towards positive values. Consequently, the system evolves from a partial wetting state to a pseudopartial configuration, and eventually achieves a complete wetting configuration. Notice how this wetting transition is qualitatively different from the one along path 1, as it involves different wetting states, and shows no hysteresis. These observations suggest at least two different ways to trigger a wetting transition in a solid-water-oil system. First, by changing the pH and salt concentration in the water phase, it is possible to affect the potential at infinite separation and the Δ parameters at the interfaces. As observed in Ref. [14], such processes indeed take place in real systems and give rise to ion adsorption-induced wetting transitions. Second, it is possible to apply a voltage between the solid substrate and the water, and thus modify its equilibrium voltage. This latter approach would provide an active control over the wetting configuration of the system. Electrowetting on dielectric (EWOD) has been extensively applied as a means to modify the contact angle of partial wetting droplets. However, it is not possible to obtain real wetting transition using electrowetting, due to the well-known phenomenon of contact angle saturation where the microscopic contact angle of the drops remains large at all times [17]. These results suggest that electrowetting on reactive substrates might access a much wider wetting

configuration space. Recent experiments by Lomax *et al.* [32] suggest that this might indeed be possible for specific graphitic substrates. One should take into account, however, that electrostatic interactions are always complemented by other interaction forces such as long-range van der Waals forces and short-range chemical (e.g., hydration) forces. As a consequence, the range of wetting scenarios and the nature of the various transitions may become even more complex. Nevertheless, compared to the other forces the range of tunability of electrostatics is arguably the widest and the most easily accessible by external control parameters. Here, we have proposed a method, which provides a trick to achieve a true electrowetting-triggered wetting transition. In the Appendix, we provide an example of a specific implementation of the ideas explained in the work for a specific set of chemical surface speciation reactions and their relation to the regulation parameter discussed above.

V. CONCLUSION

In this paper we described the electrostatic contribution to the wetting properties of oil-water-solid systems, using a linearized Poisson-Boltzmann theory in combination with a linearized charge-regulation model. We predict four distinct wetting regimes, which are functions of the potential at infinite separation and a charge regulation parameter Δ for each interface. Using these boundary parameters as input, our approach provides analytic expressions for the equilibrium contact angle in the partial wetting configurations, and the boundaries between wetting states. We observe that charge regulation relaxes the asymptotic repulsive or attractive behavior that would arise for pure constant-charge or constant-potential boundary conditions. In spite of the simplification of this linearized model, we find complex wetting transitions upon external charging of the substrates, both with and without hysteresis. Finally, we show how a typical complexation interface can be effectively described by a piecewise linear charge-regulation model.

APPENDIX: EXPLICIT CALCULATION OF Δ FROM A TWO-SPECIES COMPLEXATION MODEL

The analysis in the main text provides a detailed understanding of the electrowetting properties of an oil-water-solid system from a physical point of view. However, we would like to connect the parameters $\Delta_{1,2}, \psi_{1\infty,2\infty}$ to the surface chemistry of the interfaces, and discuss how they can be modified. We will thus consider a simple complexation model for a mica-water interface, where each surface site can bind a proton or a cation,

$$SH \rightleftharpoons S^- + H^+ \tag{A1a}$$

$$SC^{Z_c-1} \rightleftharpoons S^- + C^{Z_c}. \tag{A1b}$$

The equilibrium constant for the two processes are:

$$K_C = \frac{\{S^-\}[C^{Z_c}]}{\{SC^{Z_c-1}\}} \tag{A2a}$$

$$K_H = \frac{\{S^-\}[H^+]}{\{SH\}}, \tag{A2b}$$

where $\{A\}$ is the surface density of specie A (in sites/nm^2) and [B] is the volume density of specie B (in mole/l). As the total site density at the interface (Γ) is constant, we can write the sum of all surface concentration contributions as:

$$\{S^-\} + \{SH\} + \{SC^{Z_c-1}\} = \Gamma. \tag{A3}$$

We can use Eqs. (A2a)–(A2b) and (A3) to find the values of $\{S^-\}, \{SH\}$ and $\{SC^{(Z_c-1)+}\}$, which, in turn, provide the surface charge at the interface:

$$\sigma(\psi) = -\{S^-\} + (Z_c - 1)\{SC^{Z_c-1}\} = e\Gamma \frac{\frac{(Z_c-1)[C^{Z_c}]}{K_C} - 1}{1 + \frac{[H^+]}{K_H} + \frac{[C^{(Z_c)+}]}{K_C}}. \tag{A4}$$

The dependence on the electrostatic potential ψ in Eq. (A4) is implicit, and arises from the relation between the concentrations of cations and protons at the interface with their bulk concentrations, $[H^+]_\infty$ and $[C^{Z_c}]_\infty$, through the Boltzmann distribution:

$$[H^+] = [H^+]_\infty e^{-\frac{e\phi_s}{k_B T}} \tag{A5a}$$

$$[C^{Z_c}] = [C^{Z_c}]_\infty e^{-\frac{Z_c e\phi_s}{k_B T}}. \tag{A5b}$$

Let us analyze the asymptotic behavior of Eq. (A4). For $\psi \to +\infty$, we get $\sigma(\psi) = \sigma_{\min} = -e\Gamma$. This corresponds to $\{S^-\} = \Gamma$, i.e., all surface sites are depleted, as the large positive potential repels all cations and protons. For $\psi \to -\infty$, we have $\sigma(\psi) = \sigma_{\max} = e\Gamma(Z_c - 1)$. If $Z \geqslant 2$, all sites are thus accepting a cation, while for $Z = 1$ the substrate charge is zero. Thus, as we can see in Fig. 7(a), $\sigma(\psi)$ has a characteristic profile, with two plateaus for $\psi \to \pm\infty$, and a sharp transition in between. The inputs to the Debye-Huckel equation from this complexation model are the potential ψ_∞ and the slope $\frac{d\sigma}{d\psi}|_{\psi=\psi_\infty}$, from which the parameter Δ is easily derived. The first value is easily obtained equating Eq. (A4)

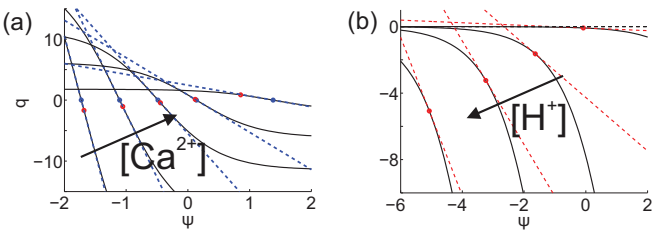

FIG. 7. (a) $q(\psi)$ profiles for the mica-water interface, for Ca^{2+} bulk concentrations between 1 and 500 mM at pH = 6. The dashed blue lines are obtained by linearizing the charge potential relation around the point of zero charge [blue (upper) dots, arising from crossing the complexation charge curve with the Grahame equation], while the red (lower) dots indicate the charge for an isolated surface, q_∞. The surface chemistry coefficients are: $\Gamma = 0.8$ sites/nm^2, $pK_H = 4$, and $pK_{Ca^{2+}} = 1.5$ (b) $q(\psi)$ profiles for the oil-water interface, for pH = 4,6,7,8, $\Gamma_{ow} = 17.3$ sites/nm^2 and $pK_{H,w} = 7$. The dashed red lines are obtained linearizing the charge potential relation around the charge at infinite separation (red dots).

and Grahame relation Eq. (4). An analytic expression,

$$\frac{d\sigma}{d\psi} = -e\Gamma \frac{\frac{[H^+]}{K_H} + Z_c^2 \frac{[C^{Z_c}]}{K_C} + (Z_c - 1)^2 \frac{[H^+]}{K_H}\frac{[C^{Z_c}]}{K_C}}{\left(1 + \frac{[H^+]}{K_H} + \frac{[C^{(Z_c)}]}{K_C}\right)^2}, \quad \text{(A6)}$$

can be easily derived from Eq. (A4) and evaluated at $\psi = \psi_\infty$, though the result is in general quite complex. Eq. (A6) simplifies dramatically if we evaluate it at the isoelectric point ψ_{iso}, for which $\sigma(\psi_{iso}) = 0$. We then get:

$$\left.\frac{d\sigma}{d\psi}\right|_{\psi=\psi_{iso}} = -e\Gamma \frac{Z_c - 1}{1 + \frac{[H^+]_\infty}{K_H} \sqrt[Z_c]{\frac{Z_c - 1}{Z_c^2}\frac{K_C}{[C^{(Z_c)}]_\infty}}}, \quad \text{(A7)}$$

Linearizing Eq. (A6) around the isoelectric point can be a rather good approximation for the intermediate behavior of amphoteric substrates. In Fig. 7(a) we plot $\sigma(\psi)$ for a mica substrate at pH = 6 and $CaCl_2$ concentration in the range 1–500 mM. We can see that the linear approximation at the isoelectric point (dashed blue line) captures very accurately the transition regime of the full $\sigma(\psi)$ curves (solid lines).

As mentioned in the main text, the oil-water interface can be described in terms of the autolysis reaction:

$$S \equiv H_2O \rightleftharpoons S \equiv OH^- + H^+ \quad \text{(A8)}$$

The expression for $\sigma(\psi)$ is easily derived analogously to what we did for the mica-water interface:

$$\sigma(\psi) = -\{S^-\} = e\Gamma_{ow} \frac{-1}{1 + \frac{[H^+]}{K_{H,w}}}. \quad \text{(A9)}$$

Notice how the the oil-water interface can only assume negative charge. Here Γ_{ow} is the water molecule density at the oil-water interface, and $K_{H,w}$ is the autolysis constant. In Fig. 7(b), we plot $\sigma(\psi)$ at the oil-water interface for pH 4,...,8, $\Gamma_{ow} = 17.3$ sites /nm^2 and $pK_{H,w} = 7$ [24]. As expected from experimental data, the charge at infinite separation becomes progressively more negative for increasing pH [30]. While in principle this $\sigma(\psi)$ curve should also exhibit a negative plateau, the large number of available sites makes the maximum negative charge very large, and in practice not relevant in most situations.

Finally, in Fig. 8 we show in green which regions of the $\sigma(\psi)$ curves are accessed when the two interfaces are brought together. This analysis allows us to assess the validity of the linearization approach, shown as dashed red lines in each plot. At pH = 3, the mica-water interface shows a charge regulation parameter $\Delta = 0.024$, while the oil-water interface exhibits constant zero charge. Both regimes are accurately captured by the linearization, and the charge does not deviate significantly from the value at infinite separation, shown as a red dot in both plots. For pH = 6 both interface show a charge-regulating behavior. The linear approximation is somewhat less accurate, but the agreement is still qualitatively good. At pH = 9, the mica-water interface moves into the positive constant-charge plateau. A piecewise linear description is necessary in this

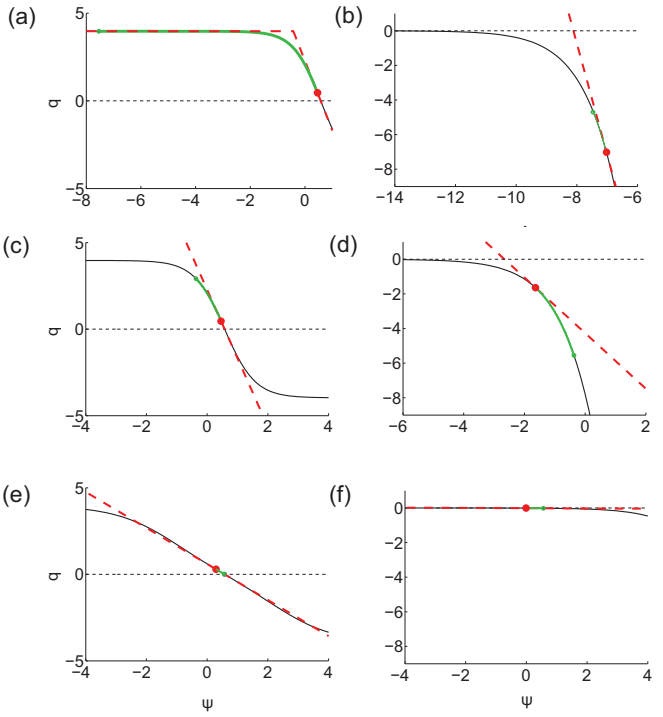

FIG. 8. $q(\psi)$ profiles for the mica water and oil-water interfaces, at (a), (b) pH = 9. (c), (d) pH = 6, and (e), (f) pH = 3. In all plots, the black curve represents the $q(\psi)$ according to Eqs. (A4) and (A9) and the red dashed line shows the linear approximation around the charge at infinite separation, shown as a red dot. The green solid line shows the change in surface charge when the interfaces are brought from infinite to zero separation.

case, employing the linearization around q_∞ for charges below the maximum value of $+e\Gamma$, and a constant-charge description for when the interfaces are drawn closer. In all these scenarios, at least one of the interfaces is charge regulating. The two substrates will then have the same potential and opposite surface charges at zero separation, thus avoiding the singularities associated to the constant-charge and the constant-potential scenarios. The generality of the approach described in this Appendix shows that our model could be extended to other solid-water-hydrophobic interface systems. One example would be a solid-water-air system. However, when compared to the oil-water interface, the air-water one will exhibit major qualitative differences, such as a different surface chemistry (complexation model) and a much larger surface tension.

A final remark concerns the bulk properties of the substrates. In our model, the solid substrate and the oil phase are only accounted for through their surface charge. However, bulk properties such as their dielectric permittivities would play a role for other interfacial forces, such as Van der Waals interactions, which we do not address in this paper.

[1] H. Butt and M. Kappl, *Surface and Interfacial Forces* (Wiley, 2009).

[2] J. Israelachvili, *Intermolecular and Surface Forces: Revised Third Edition* (Elsevier Science, 2011).

[3] D. Ben-Yaakov and D. Andelman, Phys. A **389**, 2956 (2010).
[4] R. Pashley and J. Israelachvili, J. Colloid Interface Sci. **97**, 446 (1984).
[5] J. Klein, Nature **288**, 248 (1980).
[6] A. L. Weisenhorn, P. Maivald, H.-J. Butt, and P. K. Hansma, Phys. Rev. B **45**, 11226 (1992).
[7] H.-J. Butt, Biophys. J. **60**, 1438 (1991).
[8] B. W. Ninham and V. Parsegian, J. Theor. Biol. **31**, 405 (1971).
[9] S. H. Behrens and M. Borkovec, Phys. Rev. E **60**, 7040 (1999).
[10] S. L. Carnie and D. Y. Chan, J. Colloid Interface Sci. **161**, 260 (1993).
[11] G. J. Hirasaki, Soc. Pet. Eng. **6**, 217 (1991).
[12] J. Zheng, S. H. Behrens, M. Borkovec, and S. E. Powers, Environ. Sci. Technol. **35**, 2207 (2001).
[13] G. Hanly, D. Fornasiero, J. Ralston, and R. Sedev, J. Phys. Chem. C **115**, 14914 (2011).
[14] F. Mugele, B. Bera, A. Cavalli, I. Siretanu, A. Maestro, M. Duits, M. Cohen-Stuart, D. van den Ende, I. Stocker, and I. Collins, Sci. Rep. **5**, 10519 (2015).
[15] I. Ibagon, M. Bier, and S. Dietrich, J. Chem. Phys. **138**, 214703 (2013).
[16] I. Ibagon, M. Bier, and S. Dietrich, J. Chem. Phys. **140**, 174713 (2014).
[17] F. Mugele and J.-C. Baret, J. Phys.: Condens. Matter **17**, R705 (2005).
[18] J. S. Buckley, Curr. Opin. Colloid Interface Sci. **6**, 191 (2001).
[19] A. Lager, K. Webb, C. Black, M. Singleton, K. Sorbie *et al.*, Petrophysics **49**, 28 (2008).
[20] P. C. Myint and A. Firoozabadi, Curr. Opin. Colloid Interface Sci. **20**, 105 (2015).
[21] D. McCormack, S. L. Carnie, and D. Y. Chan, J. Colloid Interface Sci. **169**, 177 (1995).
[22] P. G. de Gennes, Rev. Mod. Phys. **57**, 827 (1985).
[23] P.-G. De Gennes, F. Brochard-Wyart, and D. Quéré, *Capillarity and wetting phenomena: drops, bubbles, pearls, waves* (Springer, Berlin, 2004).
[24] J. Lützenkirchen, T. Preočanin, and N. Kallay, Phys. Chem. Chem. Phys. **10**, 4946 (2008).
[25] S. H. Behrens and M. Borkovec, J. Phys. Chem. B **103**, 2918 (1999).
[26] R. van Hal, J. Eijkel, and P. Bergveld, Adv. Colloid Interface Sci. **69**, 31 (1996).
[27] R. M. Pashley, J. Colloid Interface Sci. **83**, 531 (1981).
[28] I. Siretanu, D. Ebeling, M. P. Andersson, S. S. Stipp, A. Philipse, M. C. Stuart, D. van den Ende, and F. Mugele, Sci. Rep. **4**, 4956 (2014).
[29] M. Chaplin, Water **1**, 1 (2009).
[30] J. K. Beattie, A. M. Djerdjev, G. V. Franks, and G. G. Warr, J. Phys. Chem. B **109**, 15675 (2005).
[31] J. Lyklema, *Fundamentals of Interface and Colloid Science: Solid-Liquid Interfaces* (Elsevier Science, Amsterdam, 1995).
[32] D. Lomax, P. Kant, Y. Zou, H. Patten, A. Juel, and R. Dryfe, "Ultra-low voltage electrowetting", Droplets 2015 conference, University of Twente, 6–8 October (unpublished).